

Entanglement Thresholds of Doubly Parametric Quantum Transducers

Curtis L. Rau^{1,2,†}, Akira Kyle^{1,2,‡}, Alex Kwiatkowski^{1,2}, Ezad Shojaee,² John D. Teufel^{1,2}, Konrad W. Lehnert,^{1,2,3} and Tasshi Dennis^{1,2,*}

¹*Department of Physics, University of Colorado, Boulder, Colorado 80309, USA*

²*National Institute of Standards and Technology (NIST), Boulder, Colorado 80305, USA*

³*JILA, University of Colorado and NIST, Boulder, Colorado 80309, USA*

(Received 29 October 2021; revised 4 April 2022; accepted 6 April 2022; published 29 April 2022)

Doubly parametric quantum transducers, such as electro-optomechanical devices, show promise for providing the critical link between quantum information encoded in highly disparate frequencies such as in the optical and microwave domains. This technology would enable long-distance networking of superconducting quantum computers. Rapid experimental progress has resulted in impressive reductions in decoherence from mechanisms such as thermal noise, loss, and limited cooperativities. However, the fundamental requirements on transducer parameters necessary to achieve quantum operation have yet to be characterized. In this work we find simple, protocol-independent expressions for the necessary and sufficient conditions under which doubly parametric transducers in the resolved-sideband, steady-state limit are capable of entangling optical and microwave modes. Our analysis treats the transducer as a two-mode bosonic Gaussian channel capable of both beamsplitter-type and two-mode squeezing-type interactions between optical and microwave modes. For the beamsplitter-type interaction, we find parameter thresholds that distinguish regions of the channel's separability, capacity for bound entanglement, and capacity for distillable entanglement. By contrast, the two-mode squeezing-type interaction always produces distillable entanglement with no restrictions on temperature, cooperativities, or losses. Counterintuitively, for both interactions, we find that achieving quantum operation does not require either a quantum cooperativity exceeding one, or ground-state cooling of the mediating mode. Finally, we discuss where two state-of-the-art implementations are relative to these thresholds and show that current devices operating in either mode of operation are in principle capable of entangling optical and microwave modes.

DOI: 10.1103/PhysRevApplied.17.044057

I. INTRODUCTION

The realization of quantum transduction between the microwave frequencies of solid-state qubits and the optical wavelengths of current low-loss communications is a critical step towards building large-scale, long-distance quantum networks [1–3]. However, coherently bridging the 6 orders of magnitude separating these frequencies with minimal loss and added noise remains a technical challenge for all the various proposed and actively pursued transducer implementations [4–20]. Therefore, optical-electrical (OE) transduction will likely significantly limit the performance of near-term quantum networks. Understanding when a

transducer is not capable of supporting any possible quantum communication protocol is then a crucial step towards designing and evaluating protocols that are robust to transduction imperfections. Given the parameters describing the performance of an OE transducer (such as cooperativities, noises, and losses), we determine what thresholds need to be exceeded in order for the transducer to successfully achieve quantum operation. These thresholds then inform which parameters are limiting current devices.

Here we define the successful quantum operation of a transducer to be its ability to connect the optical and microwave domains through entanglement, which is only possible when the quantum channel describing a transducer is not separable across the OE partition. This is because a transducer whose channel is separable will never output entangled states and so any state it outputs can always be prepared by local operations separately in the optical and microwave domains with classical communication between them. Thus, this definition constitutes a necessary, but not always sufficient, condition that any OE transducer must first satisfy before it is capable of

*tasshi.dennis@nist.gov

†These authors contributed equally.

Published by the American Physical Society under the terms of the [Creative Commons Attribution 4.0 International license](#). Further distribution of this work must maintain attribution to the author(s) and the published article's title, journal citation, and DOI.

facilitating quantum communication between the optical and microwave domains. As we will show, there are some operating regions where a transducer is only capable of establishing bound (nondistillable) OE entanglement, which describes entanglement where many copies of the state cannot be reduced to a single, more highly entangled and purer state using local operation and classical communication (LOCC) alone [21]. Therefore, it is unlikely that a quantum communication protocol would be able to achieve high-fidelity quantum communication through such a transducer, even though, under this definition, it is operating in the quantum regime.

Previous work has proposed and analyzed specific protocols for faithful conversion of OE modes using various types of transducers. In the simplest protocol, the mode to be converted is sent through the port in one domain and ideally output from the port in the other domain. This scheme implicitly initializes the unused input port with vacuum while the unused output is ignored (traced over). The resulting quantum channel can always be characterized by effective loss and added noise parameters that directly determine the transduction fidelity [22]. An alternative protocol uses the OE entanglement generation capability of the transducer itself as a resource to accomplish the mode conversion via quantum teleportation [23–26]. More involved protocols introduce squeezed ancilla states to the unused input ports and homodyne measurements of the unused output ports in order to improve transduction fidelity of imperfect transducers [27]. Furthermore, allowing multiple uses of the transduction channel interspersed with single-mode unitaries can also improve transduction fidelity of imperfect transducers with reduced need for squeezing and homodyne measurement resources [28,29]. In all of these protocols, the classical average fidelity bounds for the transduced states cannot be surpassed if the transducer fails to achieve quantum operation under our definition. Thus, finding the thresholds for when a transducer achieves quantum operation will set the lower bounds for when any of these protocols can succeed or when protocols for networking remote microwave modes over optical links become limited by the transducers at each node [30–35].

In practice, OE quantum transduction can be physically implemented in a myriad of ways. Han *et al.* [3] provided a useful categorization in terms of the number of mediating modes and types of coupling between them. Our work is motivated by electro-optomechanical devices [4–8] that to date have demonstrated the highest conversion efficiency [5], although other devices have demonstrated larger bandwidth operation [15]. Electro-optomechanical transducers utilize a phononic mediating mode coupled to both the optical and microwave modes through two three-wave mixing interactions that together require both an optical and microwave pump. This effectively implements a four-wave mixing interaction between

the two pumps and two signal modes. While our model is motivated by the experimental limitations of such doubly parametric transducers (DPTs), it can also be applied to devices where the microwave mode is linearly coupled to the mediating bosonic mode at a fixed coupling rate (thus the microwave and mediating mode frequencies are degenerate). Piezo-optomechanical devices [9–13] are examples of such devices with linear coupling between the microwave resonator and mediating mechanical resonator. Both types of devices, after approximation by linearizing about the strong pump(s), can be viewed as two-port Gaussian bosonic channels. The DPT channel then implements either a beamsplitter-type or two-mode squeezing-type interaction between the itinerant microwave and optical modes when considering only the on-resonance frequency mode in the steady-state and resolved-sideband limits.

This paper is organized as follows. We start with a discussion of our DPT model and approximations in Sec. II. Next, in Sec. III A we show that the two-mode squeezing-type interaction with vacuum inputs produces distillable entanglement for all DPT device parameter values by relating it to a two-mode OE squeezed lossy state with effective squeezing and loss parameters. We then briefly discuss in Sec. III B how reducing the squeezing-type interaction to a single-mode amplification channel always results in it being entanglement breaking. Although the squeezing-type interaction always produces OE entanglement, the beamsplitter-type interaction may offer some advantages. Therefore, in Sec. IV A, we employ the Choi-Jamiołkowski isomorphism to analyze the beamsplitter-type two-mode channel, and find closed-form expressions for the DPT parameter thresholds that define regions where it is capable of producing OE distillable entanglement, only capable of producing OE bound entanglement, and never capable of entangling OE modes. Section IV B demonstrates that the entanglement-breaking thresholds for the simplest one-mode up-conversion and down-conversion channels are strictly worse than the two-mode thresholds. Finally, in Sec. V we numerically estimate where two current devices are in relation to these thresholds, finding that both devices exceed every threshold with the exception of electro-optomechanical [6,7] being entanglement breaking in up-conversion and the piezo-optomechanical [13] device being entanglement breaking in down-conversion.

II. DOUBLY PARAMETRIC TRANSDUCER MODEL

In general, the Hamiltonian describing a given physical DPT implementation will be nonlinear. However, the relatively weak experimentally achievable bare coupling rates between the mediating mode and a single photon can be enhanced with strong coherent optical and microwave pumps driving the doubly parametric interaction. In this

regime, the operator equations of motion can be safely linearized about the strong pump fields [36]. Thus, as the starting point for our study, we take the following set of linear Heisenberg-Langevin equations of motion, which capture the essential couplings that most physical DPT implementations can be reduced to [4]:

$$\dot{\hat{a}} = \left(i\Delta_a - \frac{\kappa_a}{2} \right) \hat{a} + iG_a(\hat{c} + \hat{c}^\dagger) + \sqrt{\kappa_a^c} \hat{a}_{\text{in}}^c + \sqrt{\kappa_a^e} \hat{a}_{\text{in}}^e, \quad (1a)$$

$$\dot{\hat{b}} = \left(i\Delta_b - \frac{\kappa_b}{2} \right) \hat{b} + iG_b(\hat{c} + \hat{c}^\dagger) + \sqrt{\kappa_b^c} \hat{b}_{\text{in}}^c + \sqrt{\kappa_b^e} \hat{b}_{\text{in}}^e, \quad (1b)$$

$$\begin{aligned} \dot{\hat{c}} = & - \left(i\omega_m + \frac{\gamma_m}{2} \right) \hat{c} + iG_a(\hat{a} + \hat{a}^\dagger) + iG_b(\hat{b} + \hat{b}^\dagger) \\ & + \sqrt{\gamma_m} \hat{c}_{\text{in}}^e. \end{aligned} \quad (1c)$$

Figure 1(a) illustrates the couplings in these equations of motion, where the annihilation operators \hat{a} and \hat{b} refer to the optical and microwave cavity modes, respectively, while \hat{c} refers to the mediating mode that couples to \hat{a} and \hat{b} at parametrically enhanced coupling rates of G_a and G_b , respectively. In the linearized regime, it is convenient to work in a frame rotating at the pump frequencies; thus, Δ_a and Δ_b describe the frequencies of \hat{a} and \hat{b} in terms of the detuning from their respective pump frequencies.

As these devices are not isolated systems, we use input-output theory in the above expressions to relate the internal operators to propagating and environmental operators [37]. We assume that the optical, microwave, and mediating modes couple to experimentally inaccessible environmental bath modes $\hat{a}_{\text{in,out}}^e$, $\hat{b}_{\text{in,out}}^e$, and $\hat{c}_{\text{in,out}}^e$ at rates κ_a^e , κ_b^e , and γ_m , respectively, while the optical and microwave cavities couple to itinerant input and output modes $\hat{a}_{\text{in,out}}^c$ and $\hat{b}_{\text{in,out}}^c$ at rates κ_a^c and κ_b^c , respectively. Thus, the optical and microwave cavities have linewidths of $\kappa_a = \kappa_a^c + \kappa_a^e$ and $\kappa_b = \kappa_b^c + \kappa_b^e$, respectively. We assume that the device is cooled to a temperature where the thermal occupancy of the environmental baths are negligible at the optical and microwave frequencies; however, the environment of the typically lower-frequency mediating mode is taken to have a thermal occupancy of n_{th} bosons. After accounting for all these couplings, we solve for the steady state in the frequency domain that results in a transfer function $\Xi(\omega)$ describing a unitary transformation on all itinerant frequency modes (input and output modes plus environmental modes). As expected from the assumed linear dynamics, $\Xi(\omega)$ represents a symplectic transform with terms describing beamsplitter-type and squeezing-type interactions between the optical and microwave input and output modes.

The full model contains an unwieldy number of parameters, but with several approximations, the transducer can be characterized by just five parameters. First, we only consider the itinerant optical and microwave sideband frequency modes that are on resonance with the mediating mode [$\Xi(\omega = \pm\omega_m)$ in a frame rotating about the strong pumps]. The interaction of these sidebands with the mediating mode is maximized by setting the magnitude of the relative pump detunings $\Delta_{\{a,b\}}$ to be equal to the mediating resonator's frequency, after accounting for frequency shifts due to coupling. We refer to setting a pump below its cavity resonance frequency ($\Delta_{\{a,b\}} = -\omega_m$, maximizing anti-Stokes scattering) as *red* detuned, while setting it above ($\Delta_{\{a,b\}} = +\omega_m$, maximizing Stokes scattering) is *blue* detuned. Next, we assume that the

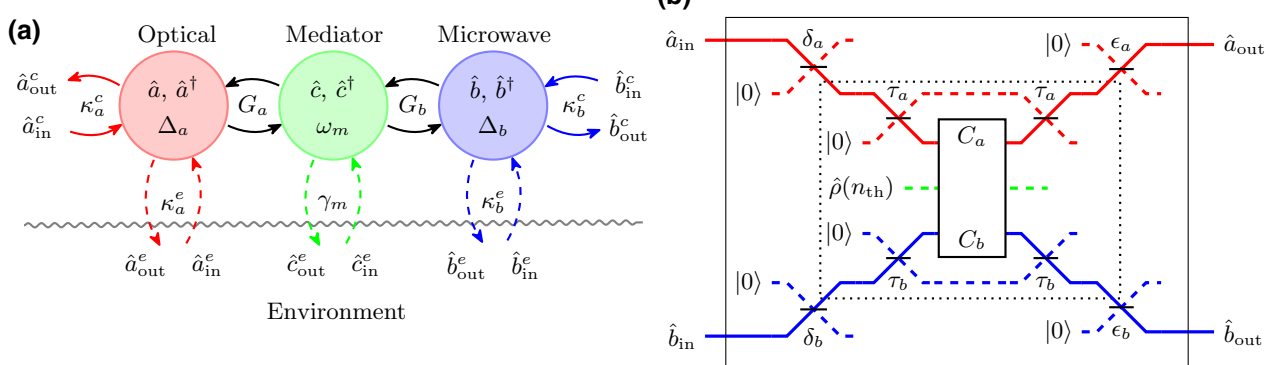


FIG. 1. (a) Diagram showing the couplings in the linearized operator equations of motion in a reference frame rotating at the pump frequencies. Circles represent internal resonator modes. (b) The equivalent circuit diagram derived from input-output relations of the central frequency mode in the resolved sideband limit. In addition to the coupling losses arising from the equations of motion, this also includes the effect of transmission losses on the itinerant optical and microwave modes. Environmental modes are represented with dashed lines. Throughout this paper we use the convention of denoting optical, microwave, and mediating modes with red, blue, and green, respectively.

mediating resonator is high Q and we make resolved sideband approximations so that $4\omega_m \gg \kappa_a, \kappa_b, \gamma_m$. This allows us to neglect the Stokes sideband when red detuned and neglect the anti-Stokes sideband when blue detuned. Thus, after these approximations, we only consider itinerant signal modes that are on resonance with their respective resonators. We then define two cooperativities as $C_i = 4G_i^2/\kappa_i\gamma_m$ where $i \in \{a, b\}$, which capture the rate at which information may be exchanged between the optical or microwave mode and the mediating mode relative to their cavity decay rates. The quantum cooperativity is then given by C_i/n_{th} . We also define $\tau_i = \kappa_i^c/\kappa_i$, where $i \in \{a, b\}$, as the cavity coupling transmissivities. Thus, we now have the five dimensionless parameters, $C_{\{a,b\}}$, $\tau_{\{a,b\}}$, and n_{th} , which characterize a DPT.

Under these approximations, the coupling transmissivity τ_i , which describes how over or under coupled the itinerant field is to the cavity field, can be modeled by an environmental mode initialized in vacuum mixing with the input and then output modes via beamsplitters, each with the same transmissivity τ_i , as shown in Fig. 1(b). We also include parameters describing losses on the input and output modes that would be “external” to the cavities. Such losses might include transmission losses, imperfect mode matching between cavity and detector modes, or any other losses that can be described by an effective beamsplitter with an environmental vacuum mode as shown in Fig. 1(b) where δ_i and ϵ_i refer to the beamsplitter transmissivities before and after the DPT, respectively, while the subscript $i \in \{a, b\}$ refers to whether it is on the optical or microwave mode, respectively.

In order to explicitly trace out the inaccessible environmental modes, we reduce the unitary $\mathbf{E}(\omega = \pm\omega_m)$ to a two-mode Gaussian channel acting on OE modes. This channel can be explicitly described by two 4×4 matrices, a unitarylike \mathbf{T} and an added noiselike \mathbf{N} , that describe the action of the channel on an arbitrary covariance matrix as $\mathbf{V} \rightarrow \mathbf{T}\mathbf{V}\mathbf{T}^\top + \mathbf{N}$ [38,39] (see Appendix A for the explicit forms). Note that we have chosen the convention of vacuum variance corresponding to 1/2 quanta for the single-frequency modes considered under our approximations.

III. SQUEEZING-TYPE INTERACTION

A. Two mode

Doubly parametric transducers implement a two-mode squeezing-type interaction between OE modes when red detuning the microwave pump while blue detuning the optical pump, or vice versa. When operated in this way, DPTs are always capable of producing distillable entanglement between OE modes. While many different OE input states can result in distillable entanglement under this interaction, it is sufficient to consider the simplest case of vacuum inputs in order to demonstrate distillable entanglement for any possible DPT parameter values. When

both OE inputs are initialized with vacuum, the covariance matrix of the resulting output state $\hat{\phi}$ is found by computing $\mathbf{V} = \mathbf{T}(\mathbf{I}_4/2)\mathbf{T}^\top + \mathbf{N}$, where \mathbf{I}_4 is the 4×4 identity matrix. A break down in our linearization about a strong pump approximation occurs when $C_i - C_j = 1$ due to terms in \mathbf{V} becoming infinite ($i, j = a, b$ when the optical pump is blue detuned and the microwave pump is red detuned, while $i, j = b, a$ in the opposite case). Therefore we exclude the region near the $C_i - C_j = 1$ pole from the following discussion of DPTs operating as squeezers. In this case of 1×1 bipartite Gaussian states, the positive partial transpose (PPT) criteria is both a necessary and sufficient condition for distillable entanglement [21,38,40]. We find that, for all parameters, $\hat{\phi}$ is entangled, and that the amount of entanglement quantified by the logarithmic negativity [41] in terms of DPT parameters is given by

$$E_N = -\log_2 \left(1 + 4 \frac{X^{(1)} - \sqrt{X^{(0)}X^{(2)}}}{(1 - C_i + C_j)^2} \right), \quad (2)$$

where, for compactness, we introduce the quantity

$$X^{(k)} = \epsilon_i \tau_i C_i (C_j + n_{\text{th}} + 1)^k + \epsilon_j \tau_j C_j (C_i + n_{\text{th}})^k.$$

We can gain additional insight into the nature of the OE entanglement by relating $\hat{\phi}$ to an effective two-mode squeezed lossy state (TMSLS) as shown in Fig. 2. A TMSLS has a specific form of the covariance matrix, which \mathbf{V} always satisfies. Solving for the TMSLS parameters of effective squeezing r' and effective OE transmissivities $\tau'_{\{a,b\}}$ respectively in terms of the DPT parameters gives

$$\cosh(r') = \frac{8(C_i + n_{\text{th}})(C_j + n_{\text{th}} + 1)}{(C_i - C_j - 1)^2} + 1, \quad (3)$$

$$\tau'_a = \tau_i \epsilon_i \frac{C_i}{C_i + n_{\text{th}}}, \quad (4)$$

$$\text{and } \tau'_b = \tau_j \epsilon_j \frac{C_j}{C_j + n_{\text{th}} + 1}. \quad (5)$$

For all nonzero $C_{\{a,b\}}$, $\tau_{\{a,b\}}$, $\epsilon_{\{a,b\}}$, and n_{th} , we see that $r' > 0$ and $0 < \tau'_a, \tau'_b < 1$, which illustrates that this state is

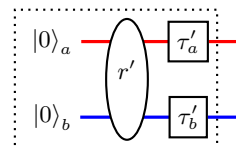


FIG. 2. Effective two-mode squeezed lossy state describing the state generated by a DPT under a squeezing-type interaction with vacuum inputs. The variable r' is the effective squeezing parameter while τ'_a and τ'_b are the effective single-mode transmissivities.

always entangled and mixed [42], and reaffirms the robustness of any TMSLS to single-mode losses [43]. Therefore, under the assumptions of our model, DPTs are always capable of entangling OE modes. However, in transforming from device parameters to effective TMSLS parameters, we see that, for large n_{th} , the $\tau'_{\{a,b\}}$ scale with n_{th}^{-1} , while conversely, r' scales with $2 \ln(n_{\text{th}})$. Thus, a device with $C_{\{a,b\}} \ll n_{\text{th}}$ would produce highly mixed entanglement from large squeezing followed by large losses.

B. Single mode

With the application of exchanging quantum information between optical and microwave frequencies in mind, an intuitive way to use a transducer is as a converter, which we define to be a one-mode channel where the input and output are at different frequencies. There are two converter classifications distinguished by the direction of information flow: (1) optical-to-microwave down-conversion [Fig. 3(a)] and (2) microwave-to-optical up-conversion [Fig. 3(b)]. There are several ways to reduce the two-mode transducer considered thus far down to one input and one output [22,24,27]. Here we examine the simplest case: initialize one mode in vacuum and trace the other mode at the output. When implementing the two-mode squeezing-type interaction, the converters become phase-insensitive phase-conjugating amplifiers (or attenuators if the loss exceeds the gain) [12]. In this configuration we find that the squeezing-type converters are always entanglement breaking [44], equivalent to a measure-and-prepare channel [45], have zero quantum capacity [21,46], and the p function of the output state is always positive [47]. However, the squeezing-type converters can function as excellent amplifiers and, for example, may be useful for amplifying classical information or reading out a microwave qubit optically.

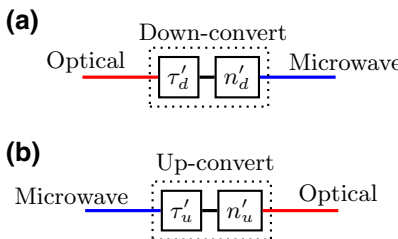


FIG. 3. (a) Single-mode down-conversion channel obtained by initializing the microwave port with vacuum and tracing out the optical output in Fig. 1(b). (b) Single-mode up-conversion channel obtained by initializing the optical port with vacuum and tracing out the microwave output in Fig. 1(b). These single-mode channels can be completely characterized by effective transmissivity $\tau'_{\{u,d\}}$ and added noise $n'_{\{u,d\}}$ parameters.

IV. BEAMSPLITTER-TYPE INTERACTION

A. Two mode

Doubly parametric transducers implement a two-mode beamsplitter-type interaction between OE modes when both pumps are red detuned. We want to know the most general conditions under which this two-mode channel can establish OE entanglement, allowing arbitrary (potentially non-Gaussian) input states with ancilla modes, operations, and measurements, all of which are separable across the optical-microwave partition. Since this interaction is not capable of intrinsically generating entanglement, it cannot entangle its OE outputs by simply initializing the inputs with vacuum as with the two-mode squeezing-type interaction. Therefore we must use a more general method for understanding the conditions under which a quantum channel is either separable or capable of entangling the modes it acts on.

In order to find such conditions, we use the Choi-Jamiołkowski (CJ) isomorphism to find the four-mode Choi state $\hat{\rho}$ that is dual to the two-mode transducer channel \mathcal{E} [48]. To calculate $\hat{\rho}$, we first define A_1 and B_1 as the respective optical and microwave modes that \mathcal{E} acts on, while A_2 and B_2 are single-mode optical and microwave continuous variable ancilla modes, respectively. Both the A_1 - A_2 and B_1 - B_2 systems are then initialized in infinitely squeezed two-mode squeezed vacuum states, and after the channel \mathcal{E} has acted on the A_1 and B_1 modes we obtain $\hat{\rho}$, as illustrated in Fig. 4 (see Appendix B for their explicit expressions). Since \mathcal{E} is Gaussian, $\hat{\rho}$ is completely characterized by a covariance matrix, which makes the following calculations tractable.

The CJ isomorphism tells us that \mathcal{E} is separable if and only if $\hat{\rho}$ is separable with respect to the bipartition defined by the A - B systems. Conversely, \mathcal{E} can facilitate entanglement creation across the A - B partition if and only if $\hat{\rho}$ is inseparable with respect to the A - B partition [49,50]. So we use the covariance matrix \mathbf{V} of the Choi state to find when \mathcal{E} is separable. By implementing the iterative method

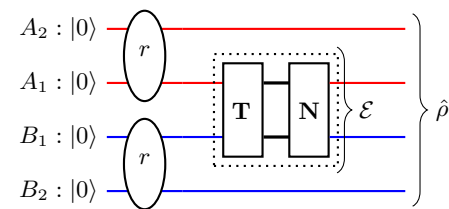


FIG. 4. Given the channel \mathcal{E} , the Choi-Jamiołkowski isomorphism gives the dual state $\hat{\rho}$, which is found by \mathcal{E} acting on inputs that are each maximally entangled with an ancilla. For continuous variable systems, the maximally entangled states are infinitely squeezed two-mode squeezed vacuum states ($r \rightarrow \infty$). The dashed box represents the two-mode channel between optical and microwave modes that the transducer implements.

for finding general Gaussian bipartite separability for an arbitrary numbers of modes [40], we numerically fit the following threshold, finding \mathcal{E} is separable with respect to the A - B partition if and only if

$$\nu_a + \nu_b \leq 1 \quad (6)$$

with

$$\nu_i = \frac{\delta_i \tau_i}{1 - \delta_i \epsilon_i (1 - 2\tau_i)^2} \left(\frac{C_i}{n_{\text{th}}} \right). \quad (7)$$

The CJ isomorphism also relates the positivity after partial transposition (PPT) criteria between a channel and its dual state. By definition, the Choi state $\hat{\rho}$ is PPT with respect to the A - B partition if and only if $\hat{\rho}^{\top_A} \geq 0$, where “ \top_A ” refers to partial transposition with respect to subsystem A . Similarly, we call the channel \mathcal{E} PPT preserving with respect to the A - B partition when, for all states $\hat{\rho}_{\text{in}}^{\top_A} \geq 0$, we have $\mathcal{E}(\hat{\rho}_{\text{in}})^{\top_A} \geq 0$. Then by the CJ isomorphism we know that \mathcal{E} is PPT preserving if and only if $\hat{\rho}$ is PPT, both with respect to the A - B partition (see Appendix C) [49–51]. So by checking the PPT criteria on \mathcal{V} (see Appendix B) we find that \mathcal{E} is PPT preserving with respect to the A - B

partition if and only if

$$\max\{\nu_a, \nu_b\} \leq 1. \quad (8)$$

Plots of these thresholds for specific parameter regions are shown in Fig. 5.

As all separable states are PPT and thus all separable channels are PPT preserving, the above thresholds given in Eqs. (6) and (8) define three distinct regions for the two-mode beamsplitter-type DPT channel.

(i) **Separable:** \mathcal{E} is separable and thus cannot be used to entangle OE modes if and only if Eq. (6) is true. Since in this region the state of the optical and microwave modes output from \mathcal{E} will never be entangled, they can always be prepared using local operations on the OE modes and classical communication between them.

(ii) **Inseparable, PPT preserving:** \mathcal{E} is inseparable and PPT preserving if and only if Eq. (8) is true and Eq. (6) is false. In this region \mathcal{E} is capable of outputting bound entangled OE states (it is, of course, still possible for separable states to be output). In order to create bound entangled Gaussian states, the input to \mathcal{E} must be locally entangled with ancillas on both the microwave and optical sides of

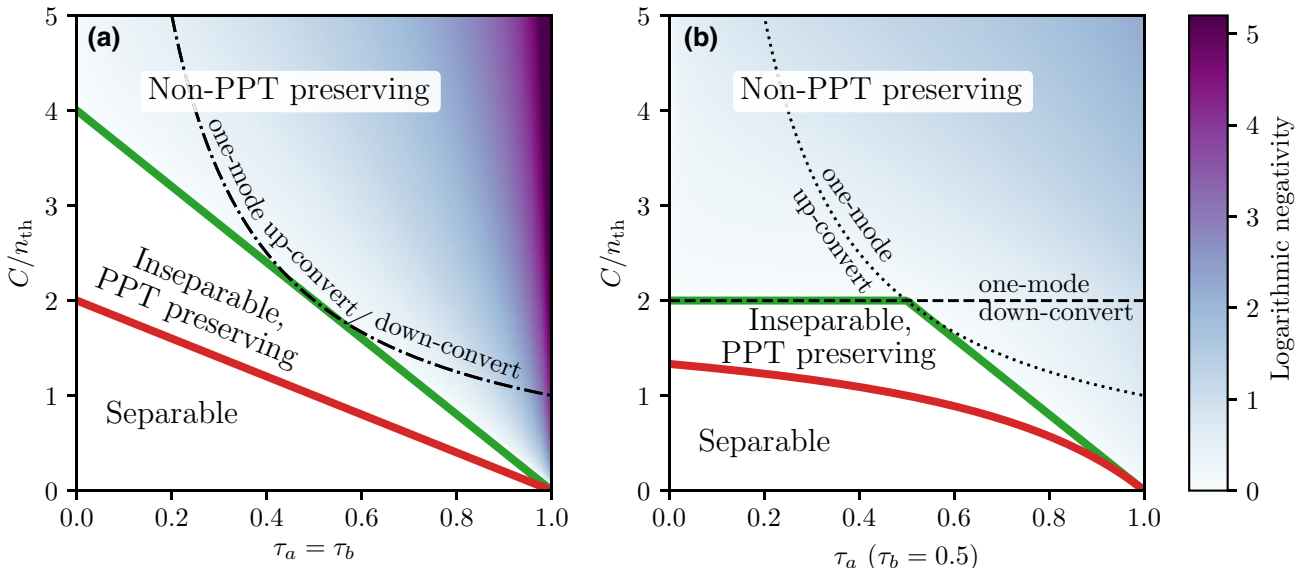


FIG. 5. Plots of entanglement thresholds for the beamsplitter-type DPT interaction with equal cooperativities ($C = C_a = C_b$) and no transmission losses ($\delta_a = \delta_b = \epsilon_a = \epsilon_b = 1$), in which case the thresholds can be characterized simply by the quantum cooperativity C/n_{th} that is related to the average thermal occupation of the mediating mode due to radiation pressure cooling [36]. (a) Thresholds as a function of equal optical and microwave coupling transmissivities. (b) Thresholds as a function of only optical transmissivity with microwave transmissivity fixed at 0.5 to illustrate the different functional behavior between the thresholds. For both plots, below the red curve the two-mode transducer channel is separable [Eq. (6)], while between the red and green curves the channel is capable of producing bound entanglement, and above the green curve the channel is capable of producing distillable entanglement [Eq. (8)]. The entanglement breaking thresholds for the one-mode up-conversion [Eq. (11)] and down-conversion [Eq. (12)] channels are indicated with the dashed curves and are never better than the two-mode transducer channel thresholds. Finally, the logarithmic negativity [41] of the transducer's Choi state is plotted, which shows increasing entanglement with higher coupling transmissivities and quantum cooperativities.

the channel because $1 \times N$ bipartite Gaussian systems cannot be bound entangled [52]. However, it may be possible to create bound-entangled non-Gaussian states without the use of ancilla modes. Additionally, in this region the beam-splitter DPT is not capable of generating entanglement that can be transferred to 1×1 OE qubit systems (since 1×1 qubit entanglement is always non-PPT [53] and LOCC is PPT preserving [21]).

(iii) **Non-PPT preserving:** \mathcal{E} is non-PPT preserving if and only if Eq. (8) is false. In this region \mathcal{E} is capable of outputting distillably entangled OE states (it is, of course, still possible for separable and bound entangled states to be output).

In this beamsplitter-type interaction, the anti-Stokes scattering processes cool the mediating mode to an equilibrium thermal occupancy of $n_m = n_{\text{th}}/(C_a + C_b + 1)$. We see that ground-state cooling ($n_m < 1$) is not necessary for the transducer channel to be either inseparable or non-PPT preserving. Additionally, devices capable of achieving high cooperativity and low loss on either the optical or microwave side, but not both, may still be capable of quantum operation despite the poorer performing side. This is a direct consequence of the non-PPT-preserving threshold given by Eq. (8) being a maximum of two expressions that each involve parameters strictly on either the optical or microwave side. However, designing experiments capable of utilizing both ports of the beamsplitter-type channel will be more challenging than simply ignoring the unused input and output ports when operating as single-mode up-conversion or down-conversion channels.

B. Single mode

We again examine the performance of a transducer when used as a single-mode converter, but now for the case when both pumps are red detuned. As before, one input is eliminated by initializing it in vacuum and one output is eliminated by tracing the output. Now the up-converter and down-converter are attenuation channels (Fig. 3), which are completely characterized by an effective transmittance $\tau'_{u/d}$ and added noise photons at the output $n'_{u/d}$ given by

$$\tau'_{\{u,d\}} = \delta_{\{b,a\}} \epsilon_{\{a,b\}} \tau_a \tau_b \frac{4C_a C_b}{(1 + C_a + C_b)^2}, \quad (9)$$

$$n'_{\{u,d\}} = \frac{1}{2} + \frac{2\epsilon_{\{a,b\}} \tau_{\{a,b\}} C_{\{a,b\}} (2n_{\text{th}} - \delta_{\{a,b\}} \tau_{\{a,b\}} C_{\{a,b\}})}{(1 + C_a + C_b)^2}. \quad (10)$$

As expected, the up-conversion and down-conversion channels both become the identity channel in the limit $n_{\text{th}} \rightarrow 0$, $C_a = C_b \rightarrow \infty$, and $\tau_{\{a,b\}}, \delta_{\{a,b\}}, \epsilon_{\{a,b\}} = 1$, and

TABLE I. Numerical estimate of entanglement thresholds for the electro-optomechanical (EM) device in Refs. [6,7] and the piezo-optomechanical (PM) device in Ref. [13]. These values correspond to the left-hand side of the respective threshold equations, where exceeding 1 indicates that the two-mode beamsplitter-type device channel is inseparable across the OE partition [Eq. (6)], non-PPT preserving across the OE partition [Eq. (8)], capable of nonentanglement breaking (non-EB) up-conversion [Eq. (11)], or capable of non-EB down-conversion [Eq. (12)]. Values that do not exceed the threshold of 1 are shown in red. All thresholds are for the beamsplitter-type interaction, since the squeezing-type interaction always produces distillable entanglement.

| Channel threshold | Equation | EM | PM |
|------------------------|----------|----------------------|----------------------|
| Inseparable | (6) | 25 | 3.4 |
| Non-PPT preserving | (8) | 25 | 3.4 |
| Non-EB up-conversion | (11) | 3.7×10^{-2} | 1.5 |
| Non-EB down-conversion | (12) | 18 | 2.8×10^{-4} |

are entanglement breaking if and only if

$$\tau_b \delta_b \frac{C_b}{n_{\text{th}}} \leq 1 \quad (\text{up-conversion}), \quad (11)$$

$$\tau_a \delta_a \frac{C_a}{n_{\text{th}}} \leq 1 \quad (\text{down-conversion}). \quad (12)$$

These thresholds follow directly from the effective loss and noise parameters [Eqs. (9) and (10)] along with the entanglement breaking criteria for one-mode channels [44]. If these inequalities are true then the converter is equivalent to a measure-and-prepare channel [45]. Therefore, Eqs. (11) and (12) are also sufficient conditions for zero quantum capacity [46]. These thresholds are more restrictive than those in the previous section [Eqs. (8) and (6)], which can be seen in Fig. 5. This is partially due to the fact that tracing over the unused output discards useful information [5]. Additionally, it is interesting to note that loss incurred after added noise due to transduction does not affect entanglement-breaking thresholds [$\epsilon_{\{a,b\}}$ does not appear in Eqs. (11) and (12)], illustrating the noncommutativity of these two sources of decoherence. Thus, it is possible to operate a transducer in a parameter regime where up-conversion is entanglement breaking while down-conversion is not, or vice versa [see Fig. 5(b)]. Finally, higher cooperativities are better for moving into the quantum regime, but once the converters are capable of quantum operation it may be necessary to strike a balance between large and equal cooperativities so that $\tau_{\{u,d\}}$ is not too small.

V. IMPLICATIONS FOR CURRENT TRANSDUCTION DEVICES

There are many promising experimental transducer implementations, so to demonstrate where current devices

are with respect to our entanglement thresholds, we numerically evaluate them for two recently demonstrated devices. One potentially advantageous way of integrating two transducers into a two-node network is to use them as up-converters and then herald entanglement with optical photon counting [32]. With this application in mind, recent experiments have integrated a qubit with either an electro-optomechanical [6] or piezo-optomechanical [13] transducer operating as an up-converter to optically measure the state of a superconducting qubit. In these experiments, the Rabi oscillations of the qubit were optically resolved via heterodyne detection in Ref. [6] and single-photon counting in Ref. [13]. These experiments are important milestones for demonstrating the compatibility of superconducting qubits with transducers; however, these experiments neither verified entangled states nor channel inseparability across the OE partition. Using the reported device parameters from these recent experiments, we can estimate whether these devices are ready for demonstrations of quantum operation by determining which thresholds they may be close to or already exceed.

We find that both devices show promise for exceeding almost every threshold in this paper. Table I summarizes the numerical estimates of the given thresholds based on the recently reported experimental parameters for the electro-optomechanical device in Refs. [6,7] and piezo-optomechanical device in Ref. [13] (see Appendix D for a discussion of how these values are estimated from the reported experimental values). Specifically, the values correspond to the left-hand side of the respective threshold equation, where a value greater than one (shown in black) indicates that the two-mode beamsplitter-type device channel is inseparable across the OE partition [Eq. (6)], non-PPT preserving across the OE partition [Eq. (8)], capable of non-EB up-conversion [Eq. (11)], or capable of non-EB down-conversion [Eq. (12)]. We see that both devices' quantum channels are potentially inseparable and non-PPT preserving since the values of the relevant thresholds all exceed one. In a one-mode up- or down-conversion operation, the asymmetry in achievable cooperativities for each device is evident. For the electro-optomechanical device, the power-dependent microwave *LC* circuit parameter noise and internal loss limited the achievable microwave cooperativity, which means that up-conversion is likely entanglement breaking in that device. For the piezo-optomechanical device, optical pump induced heating of the mechanics limited the achievable optical cooperativity, which means that down-conversion is likely entanglement breaking in that device.

Given these estimates of the thresholds for current electro-optomechanical and piezo-optomechanical devices, we conclude that their demonstrated experimental parameters are now of the sufficient order of

magnitude to achieve quantum operation. Our analysis accounts for the most significant sources of experimental imperfections; however, some limitations, such as nonzero thermal occupancy of the microwave resonator, are not accounted for in the values in Table I. A definitive experimental demonstration of quantum operation would witness optical-microwave entanglement. The squeezing-type interaction may provide a less experimentally demanding method for carrying out such a demonstration than the beamsplitter-type interaction, where an ancillary source of entanglement is necessary and thus poses integration challenges. Additionally, either interaction must overcome the experimental challenges posed by efficient filtering of the bright pumps, and noise introduced by the measurements. A potentially less demanding experiment that could infer a transducer's capability for quantum operation would involve performing Gaussian quantum channel tomography on the devices. By determining, with uncertainties, the T and N matrices that characterize the transducer's Gaussian quantum channel, the separable and PPT-preserving conditions could be evaluated via the Choi state, along with the one-mode entanglement-breaking criteria. By contrast, the reported figures of merit are typically given as values for total efficiency and added noise, which are not sufficient for evaluating all of these thresholds. Gaussian quantum channel tomography fully characterizes the transducer, giving valuable information that can be used to predict whether the device can support a given protocol, and will enable the design of better networks for connecting remote microwave systems.

VI. CONCLUSION

We find explicit thresholds on DPT parameters that must be satisfied in order for the two-mode beamsplitter-type channel to be capable of entangling OE modes. Since bound-entangled states are not useful for many quantum information tasks, we also find a more restrictive threshold that must be surpassed for the beamsplitter-type interaction to be capable of creating distillable OE entanglement. In contrast, we show that the two-mode squeezing-type interaction with vacuum inputs always creates distillable OE entanglement. Thus, we conclude that, for low cooperativity and “hot” DPTs, the squeezing-type interaction is the only viable way for such devices to achieve quantum operation. However, taking advantage of the highly mixed entangled states produced by such devices is likely technically challenging given that it is impossible to distill Gaussian states using only Gaussian operations [49,54,55]. As DPT device performance improves to below the beamsplitter-type distillable-entanglement threshold, it may be that using devices in such a

configuration offers benefits over the squeezing-type interaction. Finally, we evaluate the thresholds in this paper for two recently demonstrated transducers, finding that both devices show promise for facilitating OE distillable entanglement, especially if both inputs and outputs are utilized rather than using them as one-mode up-converters.

Current quantum information devices are based on a diverse set of physical platforms. To continue to build ever more complicated and powerful systems, we need to leverage the strengths of disparate systems. Quantum transducers capable of coherently linking disparate frequency modes will be essential components of future heterogeneous quantum networks. Yet, any transducer will introduce loss and noise into the system, which degrades their utility. Entanglement distillation, purification, concentration, or error correction protocols can help overcome the transduction imperfections; however, the entanglement thresholds found in this work must be overcome before a transducer is ready to support such protocols or be integrated into a quantum network. By employing the Choi-Jamiołkowski isomorphism we have identified fundamental thresholds that are not specific to any particular transduction protocol. These general methods can guide future research in quantum transduction beyond doubly parametric devices.

ACKNOWLEDGMENTS

The authors would like to thank Emanuel Knill, Scott Glancy, Sristy Agrawal, Ben Jamroz, and Poolad Imany for helpful suggestions and discussions. We acknowledge funding from the ARO CQTS under Grant No. 67C1098620, and the NSF under Grant No. PHYS 1734006. At the time this work was performed, C.L.R., A. Kyle, A. Kwiatkowski, and E.S. were supported as Associates in the Professional Research Experience Program (PREP) operated jointly by the NIST and the University of Colorado Boulder under Award No. 70NANB18H006 from the U.S. Department of Commerce. This is a contribution of the National Institute of Standards and Technology, not subject to U.S. copyright.

APPENDIX A: FROM INPUT-OUTPUT RELATIONS TO TWO-MODE GAUSSIAN CHANNELS

There are many different physical nonlinear Hamiltonians that can be used to perform optical-microwave transduction. Rather than starting with a specific nonlinear Hamiltonian, for generality, we start from the linearized Heisenberg-Langevin equations of motion given in Eqs. (1). These equations of motion can be compactly written as a state space model

$$\dot{\mathbf{a}}(t) = \mathbf{A}\mathbf{a}(t) + \mathbf{B}\mathbf{a}_{\text{in}}(t), \quad (\text{A1})$$

$$\mathbf{a}_{\text{out}}(t) = \mathbf{C}\mathbf{a}(t) + \mathbf{D}\mathbf{a}_{\text{in}}(t), \quad (\text{A2})$$

where

$$\mathbf{a} = [\hat{a} \quad \hat{b} \quad \hat{c} \quad \hat{a}^\dagger \quad \hat{b}^\dagger \quad \hat{c}^\dagger]^\top, \quad (\text{A3})$$

$$\mathbf{a}_{\text{in}} = [\hat{a}_{\text{in}}^c \quad \hat{a}_{\text{in}}^e \quad \hat{b}_{\text{in}}^c \quad \hat{b}_{\text{in}}^e \quad \hat{c}_{\text{in}}^e \quad (\hat{a}_{\text{in}}^c)^\dagger \quad (\hat{a}_{\text{in}}^e)^\dagger \quad (\hat{b}_{\text{in}}^c)^\dagger \quad (\hat{b}_{\text{in}}^e)^\dagger \quad (\hat{c}_{\text{in}}^e)^\dagger]^\top, \quad (\text{A4})$$

$$\mathbf{a}_{\text{out}} = [\hat{a}_{\text{out}}^c \quad \hat{b}_{\text{out}}^c \quad (\hat{a}_{\text{out}}^c)^\dagger \quad (\hat{b}_{\text{out}}^c)^\dagger], \quad (\text{A5})$$

$$\mathbf{A} = \begin{bmatrix} i\Delta_a - \kappa_a/2 & 0 & iG_a & 0 & 0 & iG_a \\ 0 & i\Delta_b - \kappa_b/2 & iG_b & 0 & 0 & iG_b \\ iG_a & iG_b & -\gamma_m/2 - i\omega_m & iG_a & iG_b & 0 \\ 0 & 0 & -iG_a & -i\Delta_a - \kappa_a/2 & 0 & -iG_a \\ 0 & 0 & -iG_b & 0 & -i\Delta_b - \kappa_b/2 & -iG_b \\ -iG_a & -iG_b & 0 & -iG_a & -iG_b & -\gamma_m/2 + i\omega_m \end{bmatrix}, \quad (\text{A6})$$

$$\mathbf{B} = \begin{bmatrix} \sqrt{\kappa_a^c} & \sqrt{\kappa_a^e} & 0 & 0 & 0 & 0 & 0 & 0 \\ 0 & 0 & \sqrt{\kappa_b^c} & \sqrt{\kappa_b^e} & 0 & 0 & 0 & 0 \\ 0 & 0 & 0 & 0 & \sqrt{\gamma_m} & 0 & 0 & 0 \\ 0 & 0 & 0 & 0 & 0 & \sqrt{\kappa_a^c} & \sqrt{\kappa_a^e} & 0 \\ 0 & 0 & 0 & 0 & 0 & 0 & \sqrt{\kappa_b^c} & \sqrt{\kappa_b^e} \\ 0 & 0 & 0 & 0 & 0 & 0 & 0 & \sqrt{\gamma_m} \end{bmatrix}, \quad (\text{A7})$$

$$\mathbf{C} = \begin{bmatrix} \sqrt{\kappa_a^c} & 0 & 0 & 0 & 0 \\ 0 & \sqrt{\kappa_b^c} & 0 & 0 & 0 \\ 0 & 0 & 0 & \sqrt{\kappa_a^c} & 0 \\ 0 & 0 & 0 & 0 & \sqrt{\kappa_b^c} \\ 0 & 0 & 0 & 0 & 0 \end{bmatrix}, \quad (\text{A8})$$

$$\mathbf{D} = \begin{bmatrix} -1 & 0 & 0 & 0 & 0 & 0 & 0 & 0 & 0 & 0 \\ 0 & 0 & -1 & 0 & 0 & 0 & 0 & 0 & 0 & 0 \\ 0 & 0 & 0 & 0 & 0 & -1 & 0 & 0 & 0 & 0 \\ 0 & 0 & 0 & 0 & 0 & 0 & -1 & 0 & 0 & 0 \end{bmatrix}. \quad (\text{A9})$$

This state space model can be transformed to the frequency-space transfer function $\Xi(\omega)$ relating the input frequency modes $\mathbf{a}_{\text{in}}(\omega)$ to the output frequency modes $\mathbf{a}_{\text{out}}(\omega)$ in the steady state:

$$\mathbf{a}_{\text{out}}(\omega) = \Xi(\omega)\mathbf{a}_{\text{in}}(\omega), \quad (\text{A10})$$

$$\Xi(\omega) = \mathbf{C}(-i\omega\mathbf{I}_6 - \mathbf{A})^{-1}\mathbf{B} + \mathbf{D}. \quad (\text{A11})$$

Here \mathbf{I}_6 is the 6×6 identity matrix.

In principle, $\Xi(\omega)$ describes the unitary evolution of the system and environmental modes; however, as the environmental modes will be traced over, their output modes are neglected in \mathbf{a}_{out} , simplifying $\Xi(\omega)$ to a rectangular 4×10 complex matrix. In order to make the rest of the analysis symbolically tractable, we apply the approximations discussed in Sec. II to get $\Xi(\omega = \pm\omega_m)$. As $\Xi(\omega = \pm\omega_m)$ preserves the canonical commutation relations of the system and environmental operators, it is a linear symplectic map, but in complex form [38,56]. For convenience, we transform $\Xi(\omega = \pm\omega_m)$ to the more standard quadrature basis symplectic form to get $\Xi^{xp}(\omega = \pm\omega_m)$, which is now defined by the vector of quadrature operators given by

$$\mathbf{a}_{\text{in}}^{xp} = [\hat{x}_{a,\text{in}}^c \quad \hat{p}_{a,\text{in}}^c \quad \hat{x}_{b,\text{in}}^c \quad \hat{p}_{b,\text{in}}^c \quad \hat{x}_{a,\text{in}}^e \quad \hat{p}_{a,\text{in}}^e \quad \hat{x}_{b,\text{in}}^e \quad \hat{p}_{b,\text{in}}^e \quad \hat{x}_{c,\text{in}}^e \quad \hat{p}_{c,\text{in}}^e]^\top, \quad (\text{A12})$$

$$\mathbf{a}_{\text{out}}^{xp} = [\hat{x}_{a,\text{out}}^c \quad \hat{p}_{a,\text{out}}^c \quad \hat{x}_{b,\text{out}}^c \quad \hat{p}_{b,\text{out}}^c]^\top. \quad (\text{A13})$$

We then reduce $\Xi^{xp}(\omega = \pm\omega_m)$ to two-mode Gaussian channels acting only on the system OE modes that are described by the unitarylike 4×4 matrix \mathbf{T} and the 4×4 noiselike matrix \mathbf{N} . We rearrange the ordering of the operators when transforming from \mathbf{a}_{in} to $\mathbf{a}_{\text{in}}^{xp}$, so now \mathbf{T} is simply given by the 4×4 matrix of the first four columns of $\Xi^{xp}(\omega = \pm\omega_m)$ defined by the system input operators. Then, \mathbf{N} is found by first taking the 4×6 matrix, which we will call \mathbf{M} , of the remaining six columns of $\Xi^{xp}(\omega = \pm\omega_m)$ defined by the environmental bath operators and then computing $\mathbf{N} = \mathbf{M}\Sigma\mathbf{M}^\top$, where $\Sigma = \mathbf{I}_6/2 + n_{\text{th}}(\mathbf{0}_4 \oplus \mathbf{I}_2)$.

The full forms of \mathbf{T} and \mathbf{N} are finally given by

$$\mathbf{T}_{\sigma_a, \sigma_b} = \frac{1}{1 - \sigma_a C_a - \sigma_b C_b} \times \begin{pmatrix} \sqrt{\delta_a \epsilon_a}[-1 + \sigma_a C_a + \sigma_b C_b + 2\tau_a(1 - \sigma_b C_b)]\mathbf{I}_2 & 2\sqrt{\epsilon_a \delta_b \tau_a \tau_b C_a C_b} \begin{pmatrix} \sigma_a & 0 \\ 0 & \sigma_b \end{pmatrix} \\ 2\sqrt{\delta_a \epsilon_b \tau_a \tau_b C_a C_b} \begin{pmatrix} \sigma_b & 0 \\ 0 & \sigma_a \end{pmatrix} & \sqrt{\delta_b \epsilon_b}[-1 + \sigma_a C_a + \sigma_b C_b + 2\tau_b(1 - \sigma_a C_a)]\mathbf{I}_2 \end{pmatrix}$$

and

$$\mathbf{N}_{\sigma_a, \sigma_b} = \frac{1}{2} \begin{pmatrix} \mu \mathbf{I}_2 & \gamma \begin{pmatrix} \sigma_a \sigma_b & 0 \\ 0 & 1 \end{pmatrix} \\ \gamma \begin{pmatrix} \sigma_a \sigma_b & 0 \\ 0 & 1 \end{pmatrix} & \nu \mathbf{I}_2 \end{pmatrix}$$

with

$$\mu = 1 - \frac{\epsilon_a \{\delta_a [1 - \sigma_a C_a - \sigma_b C_b - 2\tau_a(1 - \sigma_b C_b)]^2 - 4\tau_a C_a [1 + \sigma_a + 2n_{\text{th}} + C_b(2 + \sigma_a + \sigma_b - \delta_b \tau_b)]\}}{(1 - \sigma_a C_a - \sigma_b C_b)^2},$$

$$\nu = 1 - \frac{\epsilon_b \{\delta_b [1 - \sigma_a C_a - \sigma_b C_b - 2\tau_b(1 - \sigma_a C_a)]^2 - 4\tau_b C_b [1 + \sigma_b + 2n_{\text{th}} + C_a(2 + \sigma_a + \sigma_b - \delta_a \tau_a)]\}}{(1 - \sigma_a C_a - \sigma_b C_b)^2},$$

and

$$\gamma = \frac{2\sqrt{\epsilon_a \epsilon_b \tau_a \tau_b C_a C_b}}{(1 - \sigma_a C_a - \sigma_b C_b)^2} [4n_{\text{th}} + (\sigma_a \delta_a + \sigma_b \delta_b)(1 - \sigma_a C_a - \sigma_b C_b) + (1 - \sigma_a \sigma_b)(1 + C_a + C_b) - 2\sigma_a \delta_a \tau_a (1 - \sigma_b C_b) - 2\sigma_b \delta_b \tau_b (1 - \sigma_a C_a)],$$

where σ_a and σ_b are the signs of the optical and microwave pump detunings, respectively (-1 for red detuned, $+1$ for blue detuned).

APPENDIX B: DERIVATION OF THE PPT-PRESERVING THRESHOLD FOR THE TWO-MODE BEAMSPLITTER-TYPE INTERACTION

Here we find the constraints on transducer parameters in order for a single DPT operated with the beamsplitter-type interaction (i.e., both pumps red detuned) to facilitate the production of distillable entanglement (i.e., *NPT* states [40]) shared between optical and microwave frequency bosons. Let \mathcal{E} be the two-mode channel implemented by the beamsplitter-type interaction of a DPT (this channel is completely characterized by $\mathbf{T}_{-1,-1}$ and $\mathbf{N}_{-1,-1}$). Next, the Choi state $\hat{\rho}$ is found by initializing both the A_1 - A_2 and B_1 - B_2 systems in infinitely squeezed two-mode squeezed vacuum states, and then having the channel \mathcal{E} act on the A_1 and B_1 modes (see Fig. 4). As a consequence of the CJ isomorphism, the channel \mathcal{E} can only output states that are PPT (i.e., cannot output *NPT* states) if and only if the Choi state $\hat{\rho}$ is PPT (see Appendix C). Therefore we find the conditions under which $\hat{\rho}$ is PPT. We start by constructing the covariance matrix \mathbf{V} of the state $\hat{\rho}$, which is given by

$$\mathbf{V} = \mathbf{T}' \mathbf{V}_{\text{in}} \mathbf{T}'^{\top} + \mathbf{N}', \quad (\text{B1})$$

where from Fig. 4 we see that

$$\mathbf{T}' = \mathbf{I}_2 \oplus \mathbf{T} \oplus \mathbf{I}_2, \quad (\text{B2})$$

$$\mathbf{N}' = \mathbf{0}_2 \oplus \mathbf{N} \oplus \mathbf{0}_2, \quad (\text{B3})$$

$$\mathbf{V}_{\text{in}} = \frac{1}{2} \bigoplus_{j=1,2} \begin{pmatrix} \mathbf{I}_2 \cosh r & \mathbf{Z}_2 \sinh r \\ \mathbf{Z}_2 \sinh r & \mathbf{I}_2 \cosh r \end{pmatrix}, \quad (\text{B4})$$

and $\mathbf{T} = \mathbf{T}_{-1,-1}$ and $\mathbf{N} = \mathbf{N}_{-1,-1}$ since we are working with a beamsplitter-type transducer. Additionally, \mathbf{I}_2 and $\mathbf{0}_2$ are the 2×2 identity and zero matrices, respectively, and $\mathbf{Z}_2 = \text{diag}(1, -1)$. The CJ isomorphism requires taking $r \rightarrow \infty$; however, as we will see later, this will not in fact be necessary to do here.

The state $\hat{\rho}$ is PPT if and only if [38]

$$\tilde{\mathbf{V}} + i\Omega \geq 0, \quad (\text{B5})$$

where

$$\Omega = \frac{1}{2} \bigoplus_{j=1}^4 \begin{pmatrix} 0 & 1 \\ -1 & 0 \end{pmatrix} \quad (\text{B6})$$

and $\tilde{\mathbf{V}}$ is the partial transpose of \mathbf{V} with respect to the optical modes A_1, A_2 , given by

$$\tilde{\mathbf{V}} = \mathbf{P} \mathbf{V} \mathbf{P}^{\top}, \quad (\text{B7})$$

where $\mathbf{P} = \mathbf{Z}_2 \oplus \mathbf{Z}_2 \oplus \mathbf{I}_4$ and \mathbf{I}_4 is the 4×4 identity matrix.

Nominally, conditions under which $\hat{\rho}$ is PPT can be found by using Eq. (B5). This would be done by finding the eigenvalues $\{\lambda_i\}$ of the matrix $\tilde{\mathbf{V}} + i\Omega$ and requiring $\lambda_i \geq 0$ for all i . Stated explicitly

$$\{\lambda_i \geq 0 \mid \det(\tilde{\mathbf{V}} + i\Omega - \lambda_i \mathbf{I}_8) = 0\}. \quad (\text{B8})$$

However, since the eigenvalues are the zeros of the eighth-order characteristic polynomial, this method returns unwieldy expressions for λ_i that are difficult to simplify. An alternative method, which is computationally simpler, is to first find the boundary between PPT and *NPT* regions and then to identify the PPT and *NPT* sides.

We start by finding the conditions on the physical parameters that cause one or more of the eigenvalues to be zero. This is true if and only if the determinant is zero, so the boundary is defined by the equation

$$\det(\tilde{\mathbf{V}} + i\Omega) = 0. \quad (\text{B9})$$

Upon solving this equation for n_{th} we find that there are two solutions, i.e.,

$$n_{\text{th}} = \frac{\delta_i \tau_i C_i}{1 - \delta_i \epsilon_i (1 - 2\tau_i)^2}, \quad i = a, b, \quad (\text{B10})$$

or, alternatively, $v_i = 1$, where

$$v_i = \frac{\delta_i \tau_i}{1 - \delta_i \epsilon_i (1 - 2\tau_i)^2} \left(\frac{C_i}{n_{\text{th}}} \right). \quad (\text{B11})$$

We find that, when $v_a, v_b > 1$, two eigenvalues are negative; when $\min\{v_a, v_b\} \leq 1 < \max\{v_a, v_b\}$, a single eigenvalue is negative; and when $v_a, v_b \leq 1$, none of the

eigenvalues are negative. Therefore, $\hat{\rho}$ is PPT and \mathcal{E} is PPT preserving if and only if

$$\max\{v_a, v_b\} \leq 1. \quad (\text{B12})$$

Note that we did not need to take the limit $r \rightarrow \infty$ because the threshold is independent of r (provided that $r \neq 0$).

APPENDIX C: A CHANNEL IS PPT PRESERVING IF AND ONLY IF ITS CHOI STATE IS PPT

In this section we prove a slight generalization of Proposition (iii) of Ref. [50]. Let us consider a completely positive map (i.e., channel) \mathcal{E} acting on systems A_1 and B_1 , while implicitly understanding it to act as the identity on all other modes. Let $E_{A_1 A_2, B_1 B_2}$, acting on $\mathcal{H}_{A_1} \otimes \mathcal{H}_{A_2} \otimes \mathcal{H}_{B_1} \otimes \mathcal{H}_{B_2}$ [where $\dim(H_{A_i}) = \dim(H_{B_i}) = d$], be the Choi state of \mathcal{E} that is defined as [49,50]

$$E_{A_1 A_2, B_1 B_2} = \mathcal{E}(|\Psi\rangle \langle \Psi|_{A_1 A_2} \otimes |\Psi\rangle \langle \Psi|_{B_1 B_2}), \quad (\text{C1})$$

where $|\Psi\rangle$ is the maximally entangled state defined as

$$|\Psi\rangle_{XY} = \frac{1}{\sqrt{d}} \sum_{i=1}^d |i\rangle_X \otimes |i\rangle_Y \quad (\text{C2})$$

and $\{|i\rangle\}_{i=1}^d$ is an orthonormal basis. Finally, we define the additional systems A' and B' with $\dim(\mathcal{H}_{A'_i}) = \dim(\mathcal{H}_{B'_i}) = d'$ so that we can write a density operator $\rho_{A_1 A' B_1 B'}$ acting on $\mathcal{H}_{A_1} \otimes \mathcal{H}_{A'} \otimes \mathcal{H}_{B_1} \otimes \mathcal{H}_{B'}$ that will have modes the channel \mathcal{E} acts on while containing arbitrary modes in systems A' and B' that \mathcal{E} acts as identity on. We also define systems A'' and B'' similarly to A' and B' .

Now we can write down the statement that we will prove, where “ ${}^T X$ ” refers to partial transposition with respect to subsystem X .

For all $\rho_{A_1 A' B_1 B'}^{{}^T A_1 A'} \geq 0$, we have $\mathcal{E}(\rho_{A_1 A' B_1 B'})^{{}^T A_1 A'} \geq 0$ if and only if $E_{A_1 A_2, B_1 B_2}^{{}^T A_1 A_2} \geq 0$.

The forward implication is trivial to show since we can write $\rho_{A_1 A' B_1 B'} = |\Psi\rangle \langle \Psi|_{A_1 A_2} \otimes |\Psi\rangle \langle \Psi|_{B_1 B_2}$, where we let $A_2 B_2$ and $A' B'$ refer to the same ancillary system. In order to prove the reverse implication we need the following relation that one can readily show:

$$\begin{aligned} \mathcal{E}(\rho_{A_1 A' B_1 B'}) &= d^2 d'^2 \text{tr}_{A_2 A'' B_2 B''} (E_{A_1 A_2, B_1 B_2} |\Psi\rangle \langle \Psi|_{A' A''} \\ &\quad \times |\Psi\rangle \langle \Psi|_{B' B''} \rho_{A_2 A'', B_2 B''}^{{}^T A_2 A'' B_2 B''}). \end{aligned} \quad (\text{C3})$$

Immediately following from the above relation we have

$$\begin{aligned} \mathcal{E}(\rho_{A_1 A' B_1 B'})^{{}^T A_1 A'} &= d^2 d'^2 \text{tr}_{A_2 A'' B_2 B''} (E_{A_1 A_2, B_1 B_2}^{{}^T A_1 A_2} \\ &\quad \times |\Psi\rangle \langle \Psi|_{A' A''} |\Psi\rangle \langle \Psi|_{B' B''} \rho_{A_2 A'', B_2 B''}^{{}^T B_2 B''}). \end{aligned} \quad (\text{C4})$$

Now if we consider an arbitrary $|\psi\rangle_{A_1 A', B_1 B'} \in \mathcal{H}_{A_1 A', B_1 B'}$, we get

$$\begin{aligned} &\langle \psi |_{A_1 A', B_1 B'} \mathcal{E}(\rho_{A_1 A' B_1 B'})^{{}^T A_1 A'} |\psi\rangle_{A_1 A', B_1 B'} \\ &= d^2 d'^2 \text{tr}[(E_{A_1 A_2, B_1 B_2}^{{}^T A_1 A_2} |\Psi\rangle \langle \Psi|_{A' A''} |\Psi\rangle \langle \Psi|_{B' B''}) \\ &\quad \times (\rho_{A_2 A'', B_2 B''}^{{}^T B_2 B''} |\psi\rangle \langle \psi|_{A_1 A', B_1 B'})]. \end{aligned} \quad (\text{C5})$$

Recall that, for any $\mathbf{M} \geq 0$ and $\mathbf{N} \geq 0$, we have $\mathbf{M} \otimes \mathbf{N} \geq 0$ and $\text{tr}(\mathbf{M}\mathbf{N}) \geq 0$. Therefore, Eq. (C5) is non-negative, and so we conclude that $\mathcal{E}(\rho_{A_1 A' B_1 B'})^{{}^T A_1 A'} \geq 0$.

It is also worth stating the Choi-Jamiołkowski isomorphism in this more general context with additional, arbitrary ancilla modes

$$\begin{aligned} \mathcal{E}(\rho_{A_1 A' B_1 B'}) &= d^4 \text{tr}_{A_2 A_3 B_2 B_3} (E_{A_1 A_2, B_1 B_2} \rho_{A_3 A' B_3 B'} |\Psi\rangle \\ &\quad \times \langle \Psi|_{A' A''} |\Psi\rangle \langle \Psi|_{B' B''}). \end{aligned} \quad (\text{C6})$$

The interpretation of this equation is the same as in Ref. [50], namely if we have the Choi state $E_{A_1 A_2, B_1 B_2}$, we can always (probabilistically) simulate the action of \mathcal{E} on the $A_1 B_1$ subsystem $\rho_{A_1 A' B_1 B'}$ via the joint projection of the $A_2 A_3$ subsystem onto the maximally entangled state while doing the same for the $B_2 B_3$ subsystem.

Note that our notion of PPT-preserving channels is equivalent to the definition of completely PPT-preserving channels in [51] where they also give a proof that a channel is completely PPT preserving if and only if its Choi state is PPT with respect to the appropriate bipartition. Proposition (iii) of Ref. [50] lacked complete positivity that is necessary for the forward implication to hold, where a simple counterexample is that of the swap operator between systems A and B . Finally, note that while this proof, along with those given in Refs. [50,51], assumed finite-dimensional Hilbert spaces of dimension d , it is expected to hold as $d \rightarrow \infty$ for Gaussian states and channels due to the CJ formalism for bosonic Gaussian systems established in Refs. [48,57].

APPENDIX D: ESTIMATION OF CURRENT DEVICE PARAMETERS

In this section, we discuss details of the numerical estimation of the thresholds in Table I that are directly calculated from the parameter values given in Table IV. The values in Table IV are in turn calculated from the reported experimental values summarized in Table II for the electro-optomechanical (EM) device and Table III for the piezo-optomechanical (PM) device. Both devices suffer some amount of pump-power-dependent thermal noise that ultimately limits the maximum achievable cooperativities. Our analysis can account for pump-power-dependent thermal noise in the mediating mode by considering an

TABLE II. Experimentally measured values for the electro-optomechanical transducer in Refs. [6,7]. These values are used in Table IV to compute values for the parameters that we work with in this paper. The values in Table IV are then used to compute the numerical estimates of our thresholds given in Table I of the main text. The symbols given are those used in Refs. [6,7], not the symbols used in this paper.

| Parameter | Symbol | Value |
|---------------------------------------|------------------------------|-----------|
| Mechanical resonant frequency | $\omega_m/2\pi$ | 1.451 MHz |
| Intrinsic mechanical dissipation rate | $\gamma_m/2\pi$ | 113 mHz |
| Optical cavity external coupling | $\kappa_{o,\text{ext}}/2\pi$ | 2.12 MHz |
| Optical cavity linewidth | $\kappa_o/2\pi$ | 2.68 MHz |
| Microwave circuit external coupling | $\kappa_{e,\text{ext}}/2\pi$ | 1.42 MHz |
| Microwave circuit linewidth | $\kappa_e/2\pi$ | 1.64 MHz |
| Optomechanical coupling rate | $\Gamma_o/2\pi$ | 3 kHz |
| Electromechanical coupling rate | $\Gamma_e/2\pi$ | 14 Hz |
| Bidirectional modematching | ϵ | 0.88 |
| Microwave transmission loss | η_{mic} | 0.34 |
| Occupancy of mechanical thermal bath | n_{th} | 1000 |

elevated thermal occupancy of the environmental bath coupled to the mediating mode. However, for both the PM and EM devices, there is some amount of pump-power-dependent thermal noise introduced to the microwave resonator, which would correspond to nonzero thermal occupancy of the environmental bath coupled to the microwave resonator in our model. Given that our analysis assumes that this bath is at zero temperature, a value in Table I exceeding one does not imply that the actual device exceeded the corresponding threshold. Furthermore, it is possible that this additional source of thermal noise means that the squeezing-type interaction will not always create distillable entanglement in these devices. In other words, when the microwave environment has nonzero thermal occupancy, violation of the thresholds given in this paper are necessary (but they may not be sufficient) for quantum operation.

Table II gives the experimentally measured parameter values for the electro-optomechanical transducer in Refs. [6,7]. Pump-power-dependent heating of the microwave resonator limited the electromechanical and optomechanical coupling rates that could be realized before the microwave resonator was no longer in the ground state. We choose an optomechanical coupling rate of 3 kHz and electromechanical coupling rate of 14 Hz that together would limit the pump-induced heating of the microwave resonator to less than 0.2 thermal photons [see Fig. 4 and Fig. 10(b) of Ref. [7]]. The microwave resonator also suffered a microwave pump-power-dependent loss; however, at a 14 Hz electromechanical coupling rate, this effect is negligible and so the total linewidth of the microwave resonator is 1.64 MHz. Finally, we note that our analysis assumes well-resolved sidebands; however,

TABLE III. Experimentally measured values for the piezo-optomechanical transducer in Ref. [13]. These values are used in Table IV to compute values for the parameters that we work with in this paper. The values in Table IV are then used to compute the numerical estimates of our thresholds given in Table I of the main text. The symbols given are those used in Ref. [13], not the symbols used in this paper.

| Parameter | Symbol | Value |
|-------------------------------------|---|-----------|
| Mechanical resonant frequency | $\omega_m/2\pi$ | 5.159 GHz |
| Intrinsic mech. dissipation rate | $\kappa_{m,T1}/2\pi$ | 446 kHz |
| Optical cavity external coupling | $\kappa_{e,o}/2\pi$ | 0.81 GHz |
| Optical cavity internal coupling | $\kappa_{i,o}/2\pi$ | 0.80 GHz |
| Qubit lifetime | $T_{1,q}$ | 522 ns |
| Qubit circuit linewidth | $\kappa_q/2\pi =$ $1/(2\pi T_{1,q})$ | 305 kHz |
| Optomechanical coupling rate | $\gamma_{\text{om}}/2\pi$ | 19 kHz |
| Piezomechanical coupling rate | $g_{\text{pe}}/2\pi$ | 2.24 MHz |
| Fiber-to-device coupling efficiency | η_{cplr} | 0.65 |
| Qubit-mechanical swap efficiency | η_{swap} | 0.75 |
| Average mechanical mode occupancy | n_m | 0.43 |

this device does not operate far in the resolved sideband regime ($4\omega_m/\kappa_e \approx 2.2$ and $4\omega_m/\kappa_e \approx 3.5$).

Table III gives the experimentally measured parameter values for the piezo-optomechanical transducer in Ref. [13]. With the exception of κ_q , all values in this table are taken directly from Ref. [13]. As piezo-optomechanical devices operate with only an optical pump, the microwave-mechanical coupling rate is a fixed value dictated by the device's design. While this piezo-optomechanical device does not perfectly map onto our model, we make certain choices here in order to apply the results presented in this paper to such a device. Our model assumes a microwave resonator to be coupled to the intermediary mode, while this device instead directly couples a superconducting transmon qubit to the mechanical mode. Thus, we assume that the decay rate of qubit excitations is analogous to the decay rate of excitations from a microwave resonator. So κ_q gives this linewidth calculated based on the qubit's T_1 lifetime. From this, we then calculate the microwave cooperativity based on the usual expression in the resolved sideband approximation (see Sec. II). Given that this device is designed to transduce qubit excitations instead of itinerant microwave fields, we set the microwave coupling transmissivity to $\tau_b = 1$. However, we set $\delta_b = \epsilon_b = \eta_{\text{swap}}$ in order to capture the analogous loss of microwave excitations that would be incurred in reaching the mechanics. Since the optomechanical coupling rate and the mechanical mode's thermal occupancy is dependent on the pump pulse duration, we use the reported values that were used during the optical qubit-readout experiment. We then attribute this thermal occupancy of the mechanics to an effective thermal occupancy of the

TABLE IV. Summary of the device parameter values used to evaluate the thresholds in this paper (given in Table I) for the EM transducer in Refs. [6,7] and the PM transducer in Ref. [13]. The EM and PM expression columns use the symbols from Table II and Table III, respectively, while the “Our symbol” column uses the symbols we define in Sec. II of the main text.

| Our symbol | EM expression | EM value | PM expression | PM value |
|-------------------------|----------------------------------|----------|--|----------|
| C_a | Γ_o/γ_m | 26,000 | $\gamma_{\text{om}}/\kappa_{m,T1}$ | 0.043 |
| C_b | Γ_e/γ_m | 124 | $4g_{pe}^2/(\kappa_q\kappa_{m,T1})$ | 148 |
| n_{th} | n_{th} | 1000 | $n_m(C_a + C_b + 1)$ | 75 |
| τ_a | $\kappa_{o,\text{ext}}/\kappa_o$ | 0.791 | $\kappa_{e,o}/(\kappa_{e,o} + \kappa_{i,o})$ | 0.5 |
| τ_b | $\kappa_{e,\text{ext}}/\kappa_e$ | 0.866 | — | 1 |
| $\delta_a = \epsilon_a$ | ϵ | 0.88 | η_{cplr} | 0.65 |
| $\delta_b = \epsilon_b$ | η_{mic} | 0.34 | η_{swap} | 0.75 |

environmental bath coupled to the mechanics in order to compute the n_{th} parameter used in our analysis.

- [1] N. Lauk, N. Sinclair, S. Barzanjeh, J. P. Covey, M. Saffman, M. Spiropulu, and C. Simon, Perspectives on quantum transduction, *Quantum Sci. Technol.* **5**, 020501 (2020).
- [2] Y. Chu and S. Gröblacher, A perspective on hybrid quantum opto- and electromechanical systems, *Appl. Phys. Lett.* **117**, 150503 (2020).
- [3] X. Han, W. Fu, C.-L. Zou, L. Jiang, and H. X. Tang, Microwave-optical quantum frequency conversion, *Optica* **8**, 1050 (2021).
- [4] R. W. Andrews, R. W. Peterson, T. P. Purdy, K. Cicak, R. W. Simmonds, C. A. Regal, and K. W. Lehnert, Bidirectional and efficient conversion between microwave and optical light, *Nat. Phys.* **10**, 321 (2014).
- [5] A. P. Higginbotham, P. S. Burns, M. D. Urmey, R. W. Peterson, N. S. Kampel, B. M. Brubaker, G. Smith, K. W. Lehnert, and C. A. Regal, Harnessing electro-optic correlations in an efficient mechanical converter, *Nat. Phys.* **14**, 1038 (2018).
- [6] R. D. Delaney, M. D. Urmey, S. Mittal, B. M. Brubaker, J. M. Kindem, P. S. Burns, C. A. Regal, and K. W. Lehnert, Non-destructive optical readout of a superconducting qubit, [arXiv:2110.09539v1 \[quant-ph\]](https://arxiv.org/abs/2110.09539v1) (2021).
- [7] B. M. Brubaker, J. M. Kindem, M. D. Urmey, S. Mittal, R. D. Delaney, P. S. Burns, M. R. Vissers, K. W. Lehnert, and C. A. Regal, Optomechanical ground-state cooling in a continuous and efficient electro-optic transducer, [arXiv:2112.13429v1 \[quant-ph\]](https://arxiv.org/abs/2112.13429v1 [quant-ph]) (2021).
- [8] G. Arnold, M. Wulf, S. Barzanjeh, E. S. Redchenko, A. Rueda, W. J. Hease, F. Hassani, and J. M. Fink, Converting microwave and telecom photons with a silicon photonic nanomechanical interface, *Nat. Commun.* **11**, 4460 (2020).
- [9] A. Vainsencher, K. J. Satzinger, G. A. Peairs, and A. N. Cleland, Bi-directional conversion between microwave and optical frequencies in a piezoelectric optomechanical device, *Appl. Phys. Lett.* **109**, 033107 (2016).
- [10] M. Forsch, R. Stockill, A. Wallucks, I. Marinković, C. Gärtner, R. A. Norte, F. van Otten, A. Fiore, K. Srinivasan, and S. Gröblacher, Microwave-to-optics conversion using a mechanical oscillator in its quantum ground state, *Nat. Phys.* **16**, 69 (2019).
- [11] X. Han, W. Fu, C. Zhong, C.-L. Zou, Y. Xu, A. A. Sayem, M. Xu, S. Wang, R. Cheng, L. Jiang, and H. X. Tang, Cavity piezo-mechanics for superconducting-nanophotonic quantum interface, *Nat. Commun.* **11**, 3237 (2020).
- [12] W. Jiang, C. J. Sarabalis, Y. D. Dahmani, R. N. Patel, F. M. Mayor, T. P. McKenna, R. V. Laer, and A. H. Safavi-Naeini, Efficient bidirectional piezo-optomechanical transduction between microwave and optical frequency, *Nat. Commun.* **11**, 1166 (2020).
- [13] M. Mirhosseini, A. Sipahigil, M. Kalaee, and O. Painter, Superconducting qubit to optical photon transduction, *Nature* **588**, 599 (2020).
- [14] A. Rueda, W. Hease, S. Barzanjeh, and J. M. Fink, Electro-optic entanglement source for microwave to telecom quantum state transfer, *Npj Quantum Inf.* **5**, 108 (2019).
- [15] W. Hease, A. Rueda, R. Sahu, M. Wulf, G. Arnold, H. G. L. Schwefel, and J. M. Fink, Bidirectional electro-optic wavelength conversion in the quantum ground state, *PRX Quantum* **1**, 020315 (2020).
- [16] L. Fan, C.-L. Zou, R. Cheng, X. Guo, X. Han, Z. Gong, S. Wang, and H. X. Tang, Superconducting cavity electro-optics: A platform for coherent photon conversion between superconducting and photonic circuits, *Sci. Adv.* **4**, eaar4994 (2018).
- [17] T. M. Autry, S. Berweger, L. Sletten, R. P. Mirin, P. Kabos, K. Lehnert, and K. L. Silverman, in *2020 Conference on Lasers and Electro-Optics (CLEO)* (2020).
- [18] M. Weiß, D. Wigger, M. Nägele, K. Müller, J. J. Finley, T. Kuhn, P. Machnikowski, and H. J. Krenner, Optomechanical wave mixing by a single quantum dot, *Optica* **8**, 291 (2021).
- [19] L. A. Williamson, Y.-H. Chen, and J. J. Longdell, Magneto-Optic Modulator with Unit Quantum Efficiency, *Phys. Rev. Lett.* **113**, 203601 (2014).
- [20] R. Hisatomi, A. Osada, Y. Tabuchi, T. Ishikawa, A. Noguchi, R. Yamazaki, K. Usami, and Y. Nakamura, Bidirectional conversion between microwave and light via ferromagnetic magnons, *Phys. Rev. B* **93**, 174427 (2016).
- [21] R. Horodecki, P. Horodecki, M. Horodecki, and K. Horodecki, Quantum entanglement, *Rev. Mod. Phys.* **81**, 865 (2009).
- [22] E. Zeuthen, A. Schliesser, A. S. Sørensen, and J. M. Taylor, Figures of merit for quantum transducers, *Quantum Sci. Technol.* **5**, 034009 (2020).
- [23] S. Barzanjeh, D. Vitali, P. Tombesi, and G. J. Milburn, Entangling optical and microwave cavity modes by means

- of a nanomechanical resonator, *Phys. Rev. A* **84**, 042342 (2011).
- [24] S. Barzanjeh, M. Abdi, G. J. Milburn, P. Tombesi, and D. Vitali, Reversible Optical-To-Microwave Quantum Interface, *Phys. Rev. Lett.* **109**, 130503 (2012).
- [25] C. Zhong, Z. Wang, C. Zou, M. Zhang, X. Han, W. Fu, M. Xu, S. Shankar, M. H. Devoret, H. X. Tang, and L. Jiang, Proposal for Heralded Generation and Detection of Entangled Microwave-Optical-Photon Pairs, *Phys. Rev. Lett.* **124**, 010511 (2020).
- [26] C. Zhong, X. Han, H. X. Tang, and L. Jiang, Entanglement of microwave-optical modes in a strongly coupled electro-optomechanical system, *Phys. Rev. A* **101**, 032345 (2020).
- [27] M. Zhang, C.-L. Zou, and L. Jiang, Quantum Transduction with Adaptive Control, *Phys. Rev. Lett.* **120**, 020502 (2018).
- [28] H.-K. Lau and A. A. Clerk, High-fidelity bosonic quantum state transfer using imperfect transducers and interference, *Npj Quantum Inf.* **5**, 31 (2019).
- [29] M. Zhang, S. Chowdhury, and L. Jiang, Interference-based universal decoupling and swapping for multimode bosonic systems, *arXiv:2007.02385v2* [quant-ph] (2020).
- [30] K. Stannigel, P. Rabl, A. S. Sørensen, P. Zoller, and M. D. Lukin, Optomechanical Transducers for Long-Distance Quantum Communication, *Phys. Rev. Lett.* **105**, 220501 (2010).
- [31] K. Stannigel, P. Rabl, A. S. Sørensen, M. D. Lukin, and P. Zoller, Optomechanical transducers for quantum-information processing, *Phys. Rev. A* **84**, 042341 (2011).
- [32] S. Krastanov, H. Raniwala, J. Holzgrafe, K. Jacobs, M. Lončar, M. J. Reagor, and D. R. Englund, Optically Heralded Entanglement of Superconducting Systems in Quantum Networks, *Phys. Rev. Lett.* **127**, 040503 (2021).
- [33] M. Abdi, P. Tombesi, and D. Vitali, Entangling two distant non-interacting microwave modes, *Ann. Phys.* **527**, 139 (2014).
- [34] O. Černotík and K. Hammerer, Measurement-induced long-distance entanglement of superconducting qubits using optomechanical transducers, *Phys. Rev. A* **94**, 012340 (2016).
- [35] Z. qi Yin, W. L. Yang, L. Sun, and L. M. Duan, Quantum network of superconducting qubits through an optomechanical interface, *Phys. Rev. A* **91**, 012333 (2015).
- [36] M. Aspelmeyer, T. J. Kippenberg, and F. Marquardt, Cavity optomechanics, *Rev. Mod. Phys.* **86**, 1391 (2014).
- [37] A. A. Clerk, M. H. Devoret, S. M. Girvin, F. Marquardt, and R. J. Schoelkopf, Introduction to quantum noise, measurement, and amplification, *Rev. Mod. Phys.* **82**, 1155 (2010).
- [38] C. Weedbrook, S. Pirandola, R. García-Patrón, N. J. Cerf, T. C. Ralph, J. H. Shapiro, and S. Lloyd, Gaussian quantum information, *Rev. Mod. Phys.* **84**, 621 (2012).
- [39] J. Eisert and M. M. Wolf, Gaussian quantum channels, *arXiv:quant-ph/0505151v1* [quant-ph] (2005).
- [40] G. Giedke, B. Kraus, M. Lewenstein, and J. I. Cirac, Entanglement Criteria for all Bipartite Gaussian States, *Phys. Rev. Lett.* **87**, 167904 (2001).
- [41] G. Vidal and R. F. Werner, Computable measure of entanglement, *Phys. Rev. A* **65**, 032314 (2002).
- [42] J. Hoelscher-Obermaier and P. van Loock, Optimal gaussian entanglement swapping, *Phys. Rev. A* **83**, 012319 (2011).
- [43] S. Kotler, G. A. Peterson, E. Shojaee, F. Lecocq, K. Cicak, A. Kwiatkowski, S. Geller, S. Glancy, E. Knill, R. W. Simmonds, J. Aumentado, and J. D. Teufel, Direct observation of deterministic macroscopic entanglement, *Science* **372**, 622 (2021).
- [44] A. S. Holevo, Entanglement-breaking channels in infinite dimensions, *Problems Inf. Transmission* **44**, 171 (2008).
- [45] M. Horodecki, P. W. Shor, and M. B. Ruskai, Entanglement breaking channels, *Rev. Math. Phys.* **15**, 629 (2003).
- [46] D. Lercher, G. Giedke, and M. M. Wolf, Standard superactivation for gaussian channels requires squeezing, *New J. Phys.* **15**, 123003 (2013).
- [47] J. S. Ivan, K. K. Sabapathy, and R. Simon, Nonclassicality breaking is the same as entanglement breaking for bosonic gaussian channels, *Phys. Rev. A* **88**, 032302 (2013).
- [48] A. S. Holevo, The choi-jamiolkowski forms of quantum gaussian channels, *J. Math. Phys.* **52**, 042202 (2011).
- [49] G. Giedke and J. I. Cirac, Characterization of gaussian operations and distillation of gaussian states, *Phys. Rev. A* **66**, 032316 (2002).
- [50] J. I. Cirac, W. Dür, B. Kraus, and M. Lewenstein, Entangling Operations and Their Implementation Using a Small Amount of Entanglement, *Phys. Rev. Lett.* **86**, 544 (2001).
- [51] S. Khatri and M. M. Wilde, Principles of quantum communication theory: A modern approach, *arXiv:2011.04672v1* [quant-ph] (2020).
- [52] R. F. Werner and M. M. Wolf, Bound Entangled Gaussian States, *Phys. Rev. Lett.* **86**, 3658 (2001).
- [53] M. Horodecki, P. Horodecki, and R. Horodecki, Inseparable two spin-12density Matrices can be Distilled to a Singlet Form, *Phys. Rev. Lett.* **78**, 574 (1997).
- [54] J. Eisert, S. Scheel, and M. B. Plenio, Distilling Gaussian States with Gaussian Operations is Impossible, *Phys. Rev. Lett.* **89**, 137903 (2002).
- [55] L.-M. Duan, G. Giedke, J. I. Cirac, and P. Zoller, Entanglement Purification of Gaussian Continuous Variable Quantum States, *Phys. Rev. Lett.* **84**, 4002 (2000).
- [56] G. Adesso, S. Ragy, and A. R. Lee, Continuous variable quantum information: Gaussian states and beyond, *Open Syst. Inf. Dyn.* **21**, 1440001 (2014).
- [57] A. S. Holevo, Entropy gain and the choi-jamiolkowski correspondence for infinite-dimensional quantum evolutions, *Theor. Math. Phys.* **166**, 123 (2011).